Journal of Power Sources 208 (2012) 165–169

Contents lists available at SciVerse ScienceDirect

Journal of Power Sources

journal homepage: www.elsevier.com/locate/jpowsour

Short communication

Elastic behavior of crystalline Li–Sn phases with increasing Li concentration

Maria E. Stournara, Pradeep R. Guduru, Vivek B. Shenoy*

School of Engineering, Brown University, Providence, RI 02912, United States

ARTICLE INFO

Article history:
Received 31 October 2011
Received in revised form 4 February 2012
Accepted 6 February 2012
Available online 13 February 2012

Keywords:
Li_xSn alloys
Sn anodes
Young's modulus
Elastic constants
DFT
Anisotropy

ABSTRACT

We have studied the elastic properties of Li–Sn alloys as a function of Li concentration using first principle calculations. Here, we present the anisotropic elastic tensors as well as the orientation-averaged bulk, Young's and shear moduli and the Poisson's ratios for crystalline alloys. Our results demonstrate that crystal anisotropy has a significant effect on the stiffness of the material. We suggest that the bulk, shear and Young's moduli of isotropic Li_xSn alloys decrease monotonically with increasing Li concentration, resulting in elastic softening. On the other hand, highly anisotropic structures of very similar Li contents deviate from linearity indicating either elastic hardening or softening of the material. In addition to the significant role of anisotropy, our results also underscore the importance of including the concentration dependence of the elastic constants in the analysis of deformation during lithiation/delithiation of Sn anodes.

1. Introduction

As lithium batteries are driving a renaissance in electric-vehicle development, advanced energy storage systems with improved capacity, power and durability are becoming increasingly important. Among the most thoroughly-studied anode materials are silicon and graphite. Although silicon demonstrates very high theoretical charging capacity (3572 mAh g^{-1}), it also exhibits massive volume changes during lithiation/delithation, resulting in fracture and pulverization of the anode and significant degradation of the charging capacity. Currently, graphite is the most commonly used anode material in rechargeable Li-ion batteries, although its gravimetric capacity is relatively low (372 mAh g^{-1}), making it more and more critical to develop new anode materials that will combine greater energy density and durability.

As an alternative anode material for lithium-ion batteries, Sn and Sn-based alloys or composites have attracted much attention because of their excellent capacities [1–5]. Upon lithiation of Sn in a LiCl–KCl eutectic melt at 688 K, crystalline structures of Li_2Sn_5, LiSn, Li_7Sn_3, Li_5Sn_2, $Li_{13}Sn_5$ and Li_7Sn_2 will form [6]. The theoretical capacity of the richest Li compound is estimated to be 991 mAh g^{-1} [7], greatly exceeding that of carbon [8]. The feasibility of Sn-based materials as an anode of lithium-ion batteries has been extensively investigated and several issues have been identified. Among all of these, the most essential problem that needs to be addressed is the volume change of the Li_xSn-anode during the lithiation/delithiation process. Although it is known that the cyclic properties of lithium-ion batteries are markedly degraded by the volume change accompanying the lithiation/delithiation processes, to our knowledge there are no experimental or theoretical data for the values of the moduli of these alloys. This impairs the ability of analytical models to estimate deformation and failure for the whole range of compositions.

So far, in all the mathematical models of deformation and stress field during lithiation/delithiation, the intrinsic mechanical properties of electrodes, such as Young's modulus and Poisson's ratio, are constants, independent of Li concentration [9–14]. Recently, Qi et al., used first principles calculations to demonstrate that the polycrystalline Young's modulus of graphite increases linearly with Li concentration and triples when graphite is fully lithiated (LiC_6) [15]. Soon after that, Shenoy et al. computed the bulk modulus for various Li–Si crystalline and amorphous structures and found that the modulus of Si decreases linearly with Li concentration, dropping by one order of magnitude from its original value when the $Li_{15}Si_4$ phase is formed [16].

In this article, we compute the elastic constants, as well as the bulk, Young's and shear moduli and Poisson's ratio of Li_xSn crystalline phases using first principles calculations. Our results suggest that the bulk, shear and Young's moduli of isotropic Li-Sn structures decrease linearly with Li concentration. Our findings are consistent with the experimental mechanical analysis of Sn anodes by Chen et al., where the authors suggest that the hardness and elastic modulus of Sn drops significantly upon *ex situ* and *in situ* evaluation [17]. In addition, we find that the crystal anisotropy of certain Li–Sn structures with similar Li contents (Li_7Sn_3, $Li_{13}Sn_5$ and Li_7Sn_2), has

* Corresponding author. Tel.: +1 401 863 1475; fax: +1 401 863 9025.
E-mail address: Vivek_Shenoy@brown.edu (V.B. Shenoy).

0378-7753/$ – see front matter © 2012 Elsevier B.V. All rights reserved.
doi:10.1016/j.jpowsour.2012.02.022

Table 1
Crystal structure information for Li, Sn and Li_xSn alloys.

Phase	x	$y=x/(1+x)$	Space group	a	b	c	Volume	k-points
β-Sn	0.00	0.000	$I4_1/amd$	5.953	5.953	3.203	113.59	$18\times18\times10$
Li_2Sn_5	0.40	0.286	$P4/mbm$	10.366	10.366	3.149	338.33	$10\times10\times28$
LiSn	1.00	0.500	$P2/m$	6.933	4.317	4.419	126.65	$34\times20\times20$
Li_7Sn_3	2.33	0.700	$P2_1/m$	9.494	8.560	4.742	370.12	$10\times10\times20$
Li_5Sn_2	2.50	0.714	$R\bar{3}m$	3.183	3.183	19.80	383.78	$24\times24\times4$
$Li_{13}Sn_5$	2.60	0.722	$P\bar{3}m1$	4.700	4.700	17.13	328.14	$20\times20\times7$
Li_7Sn_2	3.33	0.777	$Cmmm$	9.924	9.924	4.726	654.54	$10\times10\times20$
Li	∞	1.000	$Fd\bar{3}m$	3.437	3.473	3.437	40.610	$22\times22\times22$

an essential effect on the elastic behavior of these phases, resulting either in increased elastic stiffness or in significant softening.

2. Methodology

All our calculations are performed using the Vienna Ab Initio Simulation Package (VASP) [18] with the Projector Augmented Wave (PAW) [19,20] method and the Perdew–Burke–Ernzerhof (PBE) [21] form of the generalized gradient approximation (GGA) for exchange and correlation. From convergence studies, we determined a kinetic energy cut-off of 300 eV and a Fermi smearing width of 0.05 eV. The optimized lattice parameters of the crystalline Li–Sn phases obtained from our calculations are summarized in Table 1 together with the number of irreducible k-points used for each of the Li–Sn alloy phases [22].

Crystals deform in an almost linear elastic manner at small strains. The strain energy density increment of a homogeneous and elastically deformed crystal is given by

$$dE = \sigma_{ij}\delta_{ij} \tag{2.1}$$

where σ_{ij} are the elements of stress tensor and δ_{ij} are the elements of strain tensor. In a more general form, the elastic constants can be expressed as

$$\frac{\partial^2 E}{\partial\delta_{ij}\partial\sigma_{ij}} = c_{ijkl} \tag{2.2}$$

According to Wallace [23], the internal energy of a crystal under a general strain δ_{ij} can be expressed by expanding the internal energy $E(V)$ of the deformed crystal with respect to the strain tensor, in terms of the Taylor series, as

$$E(V) = E(V_0, 0) + V_0\sum\sigma_{ij}\delta_{ij} + \frac{V_0}{2!}\sum c_{ijkl}\delta_{ij}\delta_{kl} \tag{2.3}$$

where V_0 is the volume of the unstrained crystal and $E(V_0, 0)$ is the corresponding ground state energy. In the above expression the strain tensors subscripts (ij, kl) are expressed in the Voigt notation scheme (11 = 1, 22 = 2, 33 = 3, 23 = 4, 31 = 5 and 12 = 6) [24]. It may be noted that the last equation is of the form

$$E(V) = M_0 + M_1\delta_i + M_2\delta_i^2 + \ldots \tag{2.4}$$

with $M_0 = E(V_0, 0)$, $M_1 = V_0\sigma_i$ and $M_2 = V_0c_{ii}/2$. Therefore, the second-order coefficient of a polynomial fit to strain energy density with respect to the deforming strain component should give the elastic constant for that strain

$$c_{ij} = \frac{2M_2}{V_0} \text{ for the normal strains}(i = 1\text{–}3) \tag{2.5}$$

and

$$c_{ii} = \frac{M_2}{2V_0} \text{ for the shear strains}(i = 4\text{–}6) \tag{2.6}$$

The last set of equations implies that other coefficients, M_0, M_1 and M_3 are zero and this will be the case for pure linear elastic strain. However, these coefficients may not be exactly zero in actual calculations, but can be made close to zero with extremely small strains. Therefore, small elastic strains, δ_i (i = 1–6), can be applied to the undeformed unit cell lattice at equilibrium. Elastic constants can be determined from the resulting change in energy.

In Table 1 we present the crystal lattice information, and in Table 2 the elastic constants calculated by computing the energies of the deformed unit cells. For cubic type phases, such as pure Sn, we applied isotropic distortion along the three vectors and tetragonal and orthorhombic shear, to obtain three independent elastic constants c_{11}, c_{12} and c_{44} [24]. For tetragonal Li_2Sn_5 and beta-tetragonal Sn phases, we applied six different deformation modes to obtain c_{11}, c_{12}, c_{13}, c_{33}, c_{44} and c_{66} [25]. For orthorhombic Li_7Sn_2, expansion along three high-symmetry directions, three monoclinic distortions, and three orthorhombic distortions were applied to obtain nine independent elastic constants [26]. For hexagonal Li_5Sn_2 and $Li_{13}Sn_5$, we used five different deformation modes to obtain c_{11}, c_{12}, c_{13}, c_{33} and c_{44} [27]. Finally, for the thirteen independent elastic constants of the monoclinic LiSn and Li_7Sn_3, we applied the same nine distortions performed on the orthorhombic phase and an additional four [28]. For the elastic constants to be extracted using the relevant equations, we applied very small strains ($\leq$2%). We allowed relaxation of the atomic positions in all the strained unit cells. Table 2 illustrates the values of all the elastic stiffness constants.

3. Results and discussion

While the elastic constants obtained from the DFT calculations are for single crystals, lithiated Sn anodes usually display polycrystalline micro-structures formed out of aggregation of single crystal grains rotated relative to each other. We, therefore, proceed to

Table 2
Elastic constants c_{ij} for Li, Sn and Li_xSn alloys. All quantities are in GPa.

Phase	c_{11}	c_{22}	c_{33}	c_{44}	c_{55}	c_{66}	c_{12}	c_{13}	c_{23}	c_{15}	c_{25}	c_{35}	c_{46}
Sn	73.10	73.10	88.41	22.01	22.01	26.67	58.40	34.78	34.78	–			
Li_2Sn_5	54.93	54.93	89.17	19.18	19.81	15.64	52.04	16.38	16.38	–			
LiSn	74.44	40.91	74.56	14.63	31.58	13.44	21.45	23.14	22.68	−1.22	−0.98	14.14	−0.56
Li_7Sn_3	73.55	48.83	72.18	37.31	10.94	40.94	22.93	−5.16	21.44	14.60	1.48	41.26	12.17
Li_5Sn_2	79.09	79.09	112.29	19.61	19.61	19.61	12.91	−4.2	−4.2	–			
$Li_{13}Sn_5$	73.38	73.38	101.14	18.72	18.72	18.72	14.89	−2.63	−2.63	–			
Li_7Sn_2	57.14	68.50	78.49	12.16	33.10	38.14	62.21	73.06		–			
Li	18.02	18.02	18.02	12.41	12.41	12.41	8.97	8.97	8.97	–			

Table 3
Reuss and Voigt values for bulk modulus (B), Young's modulus (E), shear modulus (G) and Poisson's ratio (ν). All moduli values are in GPa.

Phase	B_V	B_R	E_V	E_R	G_V	G_R	ν_V	ν_R
Sn	54.483	54.394	56.383	45.258	21.236	20.981	0.328	0.361
Li_2Sn_5	40.963	40.961	49.543	46.076	19.414	18.410	0.264	0.404
LiSn	36.050	33.117	50.362	44.733	20.106	17.543	0.275	0.263
Li_7Sn_3	21.022	18.152	62.331	47.503	30.985	22.325	0.258	0.163
Li_5Sn_2	24.100	22.316	45.991	40.405	19.460	16.860	0.181	0.198
$Li_{13}Sn_5$	33.577	33.057	51.901	45.779	29.948	19.879	0.193	0.219
Li_7Sn_2	16.385	15.418	27.101	22.545	11.067	8.206	0.219	0.242
Li	11.987	11.987	22.084	18.231	9.256	7.313	0.247	0.193

deduce polycrystalline properties from the computed anisotropic single crystal elastic constants. The determination of the stress or strain distribution in the assembly of a polycrystalline aggregate with respect to an external load can be established from the continuum theories based on Voigt [29] and Reuss [30]. These theories obtain effective isotropic elastic constants by averaging the anisotropic elastic constants over all possible orientations of the grains in a polycrystal. Using energy considerations, Hill [31] proved that the Voigt and Reuss moduli represent upper and lower limits of the true polycrystalline constants respectively, and suggested that a practical estimate of the elastic moduli was the arithmetic means of these extremes. In this work, we have adopted Hill's averaging procedure. Our results for both Voigt's and Reuss' values, as well as for Hill's, are presented in Tables 3 and 4.

The orientation averaged elastic constants and Poisson's ratios for the crystalline phases are plotted in Fig. 1 along with the plots of the elastic constants for amorphous structures. These quantities are plotted with respect to the Li fraction y of the alloy [16]. y can be related to x, through the expression $y = x/(1+x)$. Note that while x is the ratio of the Li atoms in the alloy compared to the number of Sn atoms, y is the ratio of the Li atoms to the total number of atoms. The advantage of using y in favor of x is that for elemental Li $x \to \infty$, while y is 1. Therefore all the alloy phases can be explored by letting y vary between 0 (Sn) and 1 (Li). A further advantage of plotting the elastic moduli with respect to the Li fraction y is that it allows us to assess the validity of the law of mixtures, which predicts a linear dependence of the computed properties with respect to y. Therefore, in order to compare the elastic properties of alloy phases with that of pure Sn and pure Li we have plotted the elastic moduli in the range $0 \le y \le 1$.

Table 4
Hill values form bulk modulus (B), Young's modulus (E), shear modulus (G) and Poisson's ratio (ν). All moduli values are in GPa.

Phase	B_H	E_H	G_H	ν_H
Sn	54.439	50.515	21.106	0.344
Li_2Sn_5	40.962	47.778	18.905	0.327
LiSn	32.552	47.698	18.780	0.270
Li_7Sn_3	19.534	54.414	26.301	0.205
Li_5Sn_2	12.191	43.115	18.113	0.189
$Li_{13}Sn_5$	33.316	48.740	24.400	0.205
Li_7Sn_2	15.897	24.712	9.965	0.239
Li	11.987	20.065	8.216	0.218

From Fig. 1, it can be seen that the bulk, shear, and Young's moduli as well as the Poisson's ratio exhibit an approximately linear dependence upon Li concentration, showing significant softening in the Li-rich phases, in agreement with previous experimental

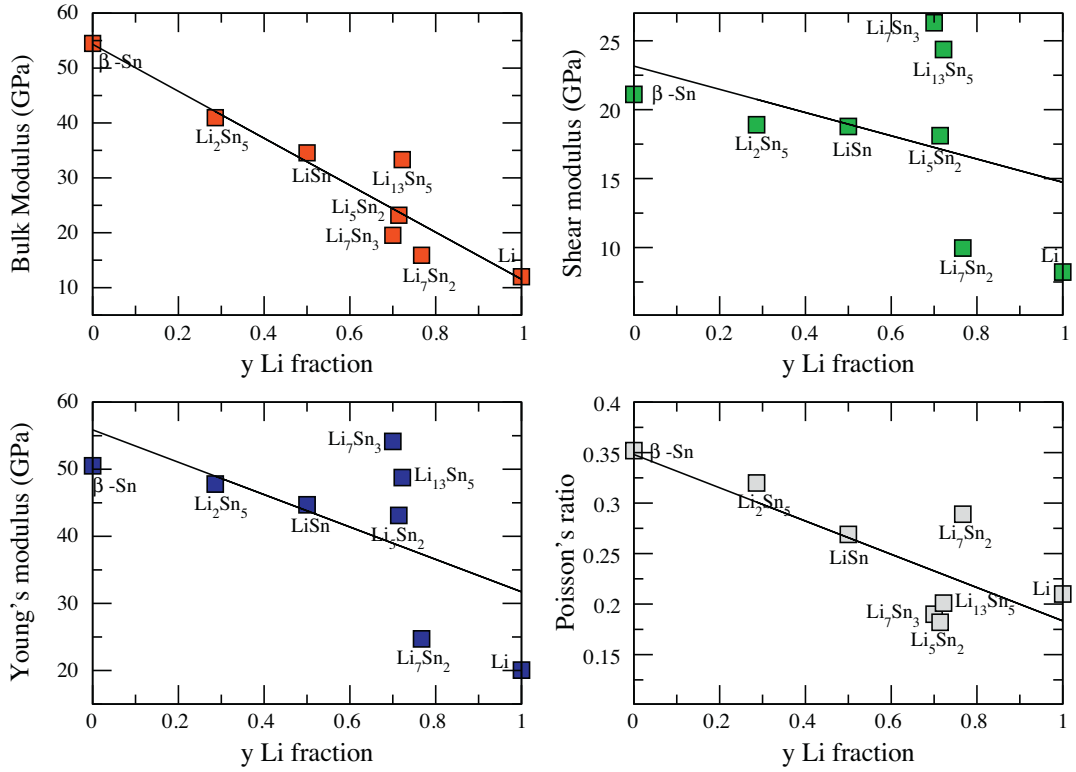

Fig. 1. Bulk modulus (B), Young's modulus (E), shear modulus (G) and Poisson's ratio (ν) versus $y = x/(x+1)$. All moduli values are in GPa.

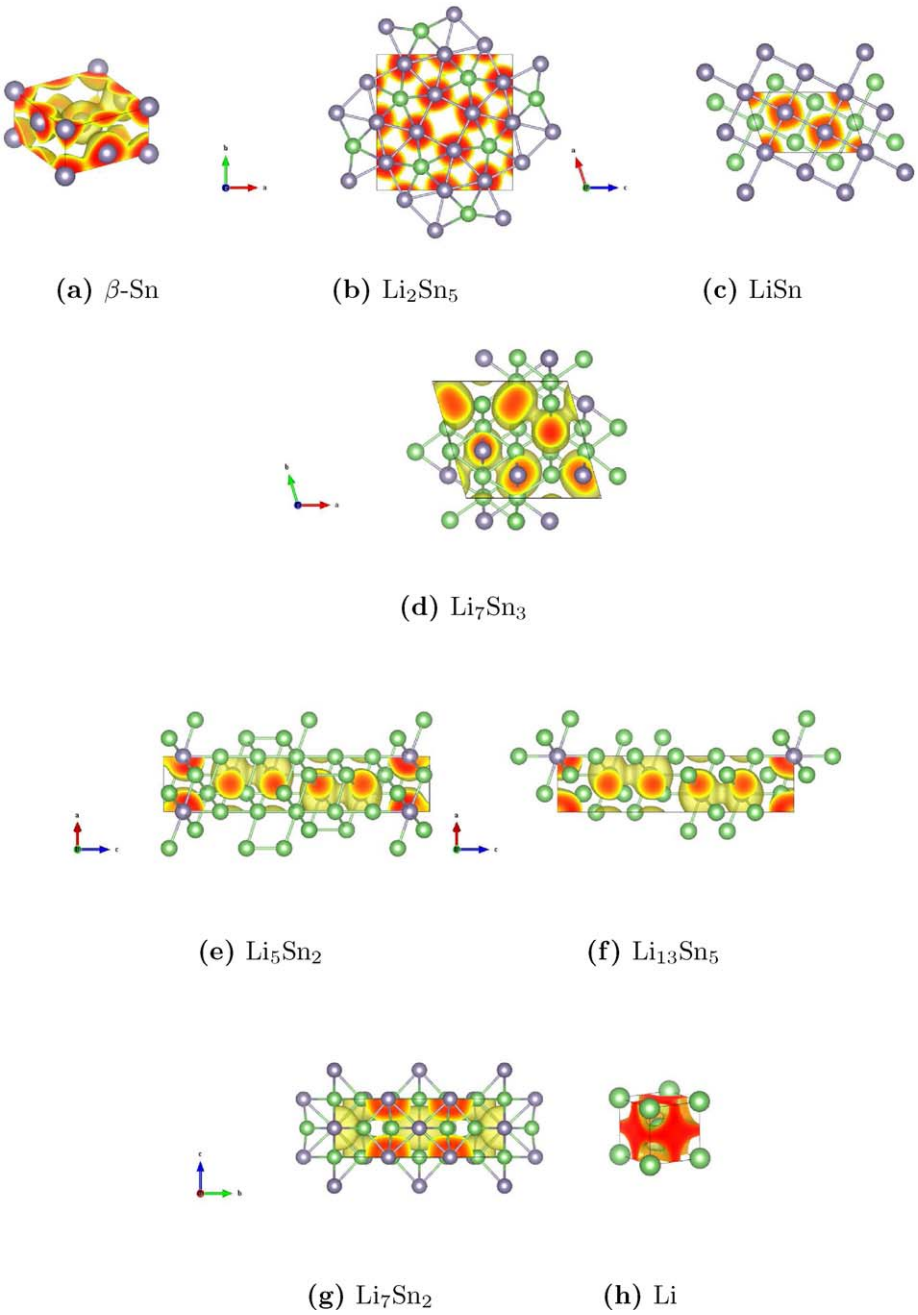

Fig. 2. Charge densities of Li_xSn alloys. The contour levels are at 0.6 bohr^{-3}. Sn atoms are represented with grey color and Li atoms with green. (For interpretation of the references to color in this figure legend, the reader is referred to the web version of the article.)

studies [17]. This monotonic decrease is interrupted around $y = 0.7$, where minimal changes in the Li content (on the order of 0.02–0.07) result in divergence from the linear trend. As demonstrated in Fig. 1, there is an 8% increase in the Young's modulus of Li_7Sn_3 in comparison to pure Sn and a 14–24% increase in the shear modulus of Li_7Sn_3 and $Li_{13}Sn_5$ phases with respect to pure Sn. In addition, for Li_7Sn_2, the Young's modulus and shear modulus drops to almost half its original Sn value, resulting in significant elastic softening. To elucidate this deviation from linearity, we calculated the crystal anisotropy indices based on the values for the bulk modulus and shear modulus computed by Voigt's and Reuss' theories.

The extent of anisotropy can be described by the universal anisotropy index A^U [32]

$$A^U = 5\frac{G_V}{G_R} + \frac{B_V}{B_R} - 6 \tag{3.1}$$

The results of the universal anisotropy indices for the Li–Sn alloys are presented in Table 5. Clearly, structures that exhibit roughly the same universal anisotropy index are equally anisotropic. In

Table 5
Calculated anisotropy factor of Li_xSn phases based on the approach adopted by Ranganathan and Ostoja-Starzewski [32].

Phase	Anisotropy factor, A^U
β-Sn	0.06
Li_2Sn_5	0.27
LiSn	0.81
Li_7Sn_3	2.09
Li_5Sn_2	0.85
$Li_{13}Sn_5$	2.54
Li_7Sn_2	1.22
Li	0.01

Table 6
Net charges of Li and Sn atoms in Li–Sn alloys computed from the PAW-PBE calculations using the Bader analysis. The calculations take into consideration both core and valence electrons.

Phase	Net charge on Li atoms	Net charge on Sn atoms
Li_2Sn_5	0.8	−0.3 to −0.5
LiSn	0.83	−0.8
Li_7Sn_3	0.8	−1.5 to −2.1
Li_5Sn_2	0.8	−2.0
$Li_{13}Sn_5$	0.8	−2.0
Li_7Sn_2	0.8	−2.5 to −3.1

agreement with what Ranganathan and Ostoja-Starzewski have suggested [32], tetragonal crystals of β-Sn and Li_2Sn_5 are elastically similar to Li cubic crystal with $A^U \approx 0$ since $(B_V/B_R) \approx 1$. Likewise, monoclinic LiSn and Li_7Sn_3 are roughly as anisotropic as Li_5Sn_2 and $Li_{13}Sn_5$, with $A^U \approx 0.82$ and $A^U \approx 2.25$ respectively. Our results demonstrate that Li_7Sn_3, $Li_{13}Sn_5$ and Li_7Sn_2 exhibit the highest values for A^U. This is consistent with the offsets observed in the monotonic decrease of the moduli presented in Fig. 1 for $y \approx 0.7$. To our knowledge, there are no previous data combining the effect of the crystal anisotropy with the elastic behavior of the Li–Sn alloys. We believe that similar trends exhibited in both theoretical [16] and experimental studies [33] for the moduli of Li_xSi alloys, can also be attributed to the anisotropy of certain Li–Si phases.

To further relate the computed elastic properties to electronic structure, we obtained the net charge on Sn atoms for each Li_xSn alloy. As shown both in Table 6 and Fig. 2, Li donates most of its electrons to Sn atoms, becoming Li-ion with a net charge of approximately +1. Sn atoms take up −1 to −4 electrons, leading to a net charge of roughly −1 to −4 compared to the crystalline β-Sn, suggesting that the nature of Li—Sn bond changes from metallic to ionic in high lithium concentration, in agreement with others [34–36]. According to previous discussions [37], the trends in moduli as a function of valence electron concentration (VEC) can be exactly understood in terms of electronic structure. Although Li—Li and Sn—Sn bond lengths are very close (i.e. 3.022 and 3.082 Å) and the bonds are metallic in both cases, Sn exhibits four times higher density of valence electrons ($5s^2\ 5p^2$), which explains the increased stiffness of Sn—Sn bond values as compared to those of Li—Li.

The charge state of Sn varies depending on the amount of Li and Sn neighboring atoms, as well as on the anisotropy of the phase. In the case of Li_7Sn_2, Sn atoms can acquire two distinct charge states depending on where they are located in the unit cell; four Sn atoms are surrounded by twelve Li atoms exhibiting −2.5 and four Sn atoms sit in an environment of fourteen Li atoms, having a charge of −3.8. Similarly, for the case Li_7Sn_3, Sn atoms surrounded by ten Li atoms are in a charge state of −1.5 while those surrounded by thirteen Li atoms possess a charge of −2.1. Charge states of Sn atoms in Li_5Sn_3 and $Li_{13}Sn_5$ phases were estimated to be −2.0. Our calculations therefore show that the elastic softening of the alloy phase is consistent with the increase in the relative population of ionic bonds of the intermediate states.

4. Conclusions

We have computed the elastic properties of Li_xSn alloys and have found that upon increase in Li concentration, the bulk, Young's and shear moduli decrease in an approximately linear matter, resulting in significant elastic softening of the most Li-rich alloys. The deviation from the linear trend is attributed to the crystal anisotropy of these phases. We believe that our results will provide a quantitative framework for the analysis of experimental measurements and that our data will provide input for mathematical models of deformation and stress field during lithiation/delithiation.

Acknowledgement

We gratefully acknowledge the support of the DOE EPSCOR-implementation grant.

References

[1] S.F. Yang, P.Y. Zavalij, M.S. Whittingham, Electrochemistry Communications 5 (2003) 587–590.
[2] R.A. Huggins, Journal of Power Sources 81 (1999) 13–19.
[3] J.O. Besenhard, J. Yang, M. Winter, Journal of Power Sources 68 (1997) 87–90.
[4] N. Tamura, R. Ohshita, M. Fujimoto, S. Fujitani, M. Kamino, I. Yonezu, Journal of Power Sources 107 (2002) 48–55.
[5] H. Mukaibo, T. Sumi, T. Yokoshima, T. Momma, T. Osaka, Electrochemical and Solid-State Letters 6 (2003) A218–A220.
[6] W. Gasior, Z. Moser, W. Zakulski, Journal of Non-Crystalline Solids 205 (1996) 379–382.
[7] L.Y. Beaulieu, D. Larcher, R.A. Dunlap, J.R. Dahn, Journal of the Electrochemical Society 147 (2000) 3206–3212.
[8] M. Winter, J.O. Besenhard, Electrochimica Acta 45 (1999) 31–50.
[9] R.A. Huggins, W.D. Nix, Ionics 6 (2000) 57–63.
[10] J. Christensen, J. Newman, Journal of the Electrochemical Society 153 (2006) A1019–A1030.
[11] J. Christensen, V. Srinivasan, J. Newman, Journal of the Electrochemical Society 153 (2006) A560–A565.
[12] X. Zhang, W. Shyy, A.M. Sastry, Journal of the Electrochemical Society 154 (2007) A910–A916.
[13] Y.-T. Cheng, M.W. Verbrugge, Journal of Power Sources 190 (2009) 453–460.
[14] Y.-T. Cheng, M.W. Verbrugge, Journal of Applied Physics 104 (2008).
[15] Y. Qi, H. Guo, L.G. Hector, A. Timmons, Journal of the Electrochemical Society 157 (2010) A558.
[16] V.B. Shenoy, P. Johari, Y. Qi, Journal of Power Sources 195 (2010) 6825–6830.
[17] J. Chen, S.J. Bull, S. Roy, H. Mukaibo, H. Nara, T. Momma, T. Osaka, Y. Shacham-Diamand, Journal of Physics D: Applied Physics 41 (2008) 025302.
[18] G. Kresse, J. Furthmuller, Physical Review B 54 (1996) 11169–11186.
[19] G. Kresse, D. Joubert, Physical Review B 59 (1999) 1758–1775.
[20] P.E. Blochl, Physical Review B 50 (1994) 17953–17979.
[21] J.P. Perdew, K. Burke, M. Ernzerhof, Physical Review Letters 77 (1996) 3865–3868.
[22] I.A. Courtney, J.S. Tse, O. Mao, J. Hafner, J.R. Dahn, Physical Review B 58 (1998) 15583–15588.
[23] D.C. Wallace, Thermodynamics of Crystals, Wiley, New York, 1972.
[24] L.D. Landau, E.M. Lifshitz, Theory of Elasticity, Butterworth-Heinemann, Oxford, 1999.
[25] X. Meng, X. Wen, G. Qin, Computation Materials Science 49 (2010) S372–S377.
[26] K.B. Panda, K.S.R. Chandran, Computation Materials Science 35 (2006) 134–150.
[27] B. Narayanan, I.E. Reimanis, J. Fuller, R. Edwin, C.V. Ciobanu, Physical Review B 81 (2010).
[28] P. Soederlind, J.E. Klepeis, Physical Review B 79 (2009).
[29] W. Voigt, Lerbuch der Kristallphysik, Taubner, Leipzig, 1928.
[30] A. Reuss, Zeitschrift fur Angewandte Mathematik und Mechanik 9 (1929) 49–58.
[31] R. Hill, Proceedings of the Physical Society of London 65 (1952) 349–354.
[32] S.I. Ranganathan, M. Ostoja-Starzewski, Physical Review Letters 101 (2008) 055504.
[33] B. Hertzberg, J. Benson, G. Yushin, Electrochemistry Communications 13 (2011) 818–821.
[34] R.A. Dunlap, D.A. Small, D.D. MacNeil, M.N. Obrovac, J.R. Dahn, Journal of Alloys and Compounds 289 (1999) 135–142.
[35] M.S. Lee, D.G. Kanhere, K. Joshi, Physical Review A 72 (2005) 1050–2947.
[36] F. Haarmann, D. Gruener, V. Bezugly, H. Rosner, Y. Grin, Zeitschrift Fur Anorganische Und Allgemeine Chemie 632 (2006) 1423–1431.
[37] J.Y. Wang, Y.C. Zhou, Physical Review B 69 (2004).